ACS chemical biology

Articles

pubs.acs.org/acschemicalbiology

Structural Flexibility of an Inhibitor Overcomes Drug Resistance Mutations in *Staphylococcus aureus* FtsZ

Junso Fujita,[†] Yoko Maeda,[†] Eiichi Mizohata,[†] Tsuyoshi Inoue,[†] Malvika Kaul,[‡] Ajit K. Parhi,[§,∥] Edmond J. LaVoie,[∥] Daniel S. Pilch,[*,‡,#] and Hiroyoshi Matsumura[*,⊥,#]

[†]Department of Applied Chemistry, Graduate School of Engineering, Osaka University, 2-1 Yamadaoka, Suita, Osaka 565-0871, Japan

[‡]Department of Pharmacology, Rutgers Robert Wood Johnson Medical School, 675 Hoes Lane, Piscataway, New Jersey 08854, United States

[§]TAXIS Pharmaceuticals, Inc., 9 Deer Park Drive, Suite J-15, Monmouth Junction, New Jersey 08852, United States

[∥]Department of Medicinal Chemistry, Ernest Mario School of Pharmacy, Rutgers University, 160 Frelinghuysen Road, Piscataway, New Jersey 08854, United States

[⊥]Department of Biotechnology, College of Life Sciences, Ritsumeikan University, 1-1-1 Noji-higashi, Shiga 525-8577, Japan

Supporting Information

ABSTRACT: In the effort to combat antibiotic resistance, inhibitors of the essential bacterial protein FtsZ have emerged as a promising new class of compounds with clinical potential. One such FtsZ inhibitor (TXA707) is associated with potent activity against clinical isolates of methicillin-resistant *Staphylococcus aureus* (MRSA) that are resistant to current standard-of-care antibiotics. However, mutations in *S. aureus* FtsZ (SaFtsZ) that confer resistance to TXA707 have been observed, with mutations in the Gly196 and Gly193 residues being among the most prevalent. Here, we describe structural studies of an FtsZ inhibitor, TXA6101, which retains activity against MRSA isolates that express either G196S or G193D mutant FtsZ. We present the crystal structures of TXA6101 in complex with both wild-type SaFtsZ and G196S mutant SaFtsZ, as well the crystal structure of TXA707 in complex with wild-type SaFtsZ. Comparison of the three structures reveals a molecular basis for the differential targeting abilities of TXA6101 and TXA707. The greater structural flexibility of TXA6101 relative to TXA707 enables TXA6101 to avoid steric clashes with Ser196 and Asp193. Our structures also demonstrate that the binding of TXA6101 induces previously unobserved conformational rearrangements of SaFtsZ residues in the binding pocket. In aggregate, the structures reported in this work reveal key factors for overcoming drug resistance mutations in SaFtsZ and offer a structural basis for the design of FtsZ inhibitors with enhanced antibacterial potency and reduced susceptibility to mutational resistance.

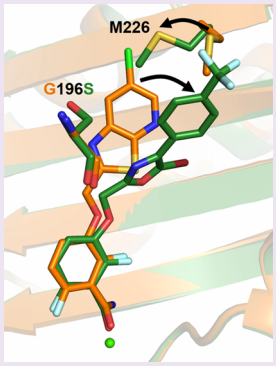

Recently, public health agencies like the World Health Organization and the Centers for Disease Control have released reports that caution an impending crisis to global public health due to the rise and spread of antibiotic resistance.[1−3] Among the pressing needs identified by these agencies to avert the crisis is the development of new antibiotics with novel bacterial targets. To this end, we recently described a novel small molecule (TXA707) that targets the bacterial protein FtsZ in *Staphylococcus aureus* (Figure 1).[4,5] FtsZ is the principal component of the Z-ring, a structure formed at midcell that is critical for cell division.[6−8] FtsZ represents an appealing new target for antibiotic development, as it is essential for bacterial survival and has not been exploited by any antibiotic in current clinical use.[9−13] Our previous studies have demonstrated that TXA707 is bactericidal against strains of *S. aureus* that are resistant to many clinically important antibiotics, including numerous subtypes of methicillin-resistant *S. aureus* (MRSA), vancomycin-resistant *S. aureus* (VRSA), linezolid-resistant *S. aureus* (LRSA), and daptomycin-resistant *S. aureus* (DRSA).[4] In addition, we have shown that a prodrug of TXA707 (TXA709) is efficacious *in*

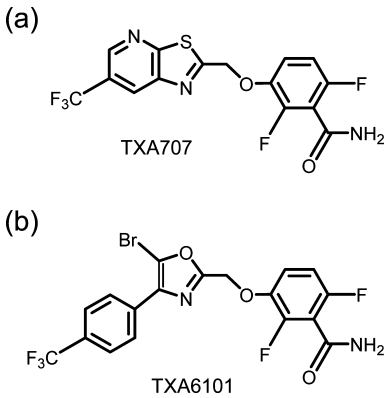

Figure 1. Chemical structures of TXA707 (a) and TXA6101 (b).

Received: April 13, 2017
Accepted: June 2, 2017
Published: June 16, 2017

DOI: 10.1021/acschembio.7b00323
ACS Chem. Biol. 2017, 12, 1947−1955

vivo in mouse models of both systemic and tissue (thigh) infections with MRSA,[4] further underscoring the potential clinical usefulness of FtsZ-targeting agents.

Two mutations in the *S. aureus ftsZ* gene that confer resistance to FtsZ-targeting agents like TXA707 are G196S and G193D, with the former being the most commonly occurring resistance mutation.[4,14−17] In this work, we describe structural studies of an FtsZ-targeting compound, TXA6101 (Figure 1), which retains activity against MRSA isolates that express either G196S or G193D mutant FtsZ protein. This compound was first reported by Stokes et al. as part of a broad structure−activity relationship study of antistaphylococcal FtsZ inhibitors with potent *in vitro* activity and favorable pharmacokinetic properties.[16,18] The difluoro-benzamide portion of TXA6101 is identical to that in TXA707. Where the two compounds are primarily different is with regard to the rotational flexibility of the five- and six-membered rings at the opposite end (Figure 1). In TXA707, the five- and six-membered rings (a thiazole and a pyridyl ring, respectively) are fused and therefore unable to rotate relative to each other. By contrast, in TXA6101, the five- and six-membered rings (an oxazole and a phenyl ring, respectively) are linked by a single bond about which both rings can freely rotate. Here, we present the crystal structures of TXA707 and TXA6101 in complex with wild-type *S. aureus* FtsZ (SaFtsZ), as well as the corresponding structure of TXA6101 in complex with the G196S mutant of SaFtsZ. These structures demonstrate how the enhanced rotational flexibility of TXA6101 enables it to target FtsZ mutants that confer resistance to TXA707. As a result of its expanded FtsZ-targeting capability, TXA6101 is associated with a lower frequency of mutational resistance in MRSA than TXA707.

RESULTS

Antibacterial Activities and Resistance Frequencies of TXA707 and TXA6101 against MRSA Isolates Expressing Wild-Type or Mutant FtsZ Proteins. We evaluated the activities of TXA707 and TXA6101 against the MRSA clinical isolate MPW020, with the resulting minimal inhibitory concentrations (MICs) being summarized in Table 1.

Table 1. Activities and Resistance Frequencies of FtsZ Inhibitors against MRSA Clinical Isolate MPW020[a]

compound	MIC (μg mL^{-1})	FOR
TXA707	1	4.3×10^{-8}
TXA6101	0.125	3.6×10^{-9}
TXD1122	4	ND

[a]MIC denotes minimal inhibitory concentration, FOR denotes frequency of resistance, and ND denotes not determined. The FOR value for TXA707 was taken from ref 5.

TXA707 is associated with an MIC of 1 μg mL^{-1}, a value in agreement with those (MIC = 0.5−2 μg mL^{-1}) we have previously reported for a range of MRSA, VRSA, LRSA, and DRSA isolates.[4] TXA6101 is 8-fold more active than TXA707, with a corresponding MIC of 0.125 μg mL^{-1}. This antistaphylococcal activity is similar to that previously reported by Stokes and co-workers for TXA6101 as well as a structurally related compound in which the linker between the oxazole and benzamide portions of the molecule is functionalized with a hydroxymethyl substituent.[16,18] To determine the role, if any, that the bromo functionality of TXA6101 plays in determining the enhanced activity of the compound, we also evaluated the MIC of a compound (TXD1122) identical to TXA6101 except that it lacks the bromo group (Supporting Information Figure S1). Significantly, the MIC of TXD1122 against MRSA MPW020 is 4 μg mL^{-1} (Table 1), 32-fold higher than the corresponding MIC of TXA6101 and 4-fold higher than the corresponding MIC of TXA707. Thus, the bromo functionality is a critical determinant of the enhanced antistaphylococcal potency of TXA6101 relative to TXA707.

We also determined the activities of TXA707 and TXA6101 against MRSA MPW020 expressing either G196S or G193D mutant FtsZ. TXA707 is inactive against both FtsZ mutant strains, with MIC values >64 μg mL^{-1} (Table 2). In striking contrast, the MIC value for TXA6101 against both mutant strains is 1 μg mL^{-1}. Previous studies have reported an MIC value of 4 μg mL^{-1} for TXA6101 (as well as its hydroxymethyl substituted analogue) against *S. aureus* expressing G196A mutant FtsZ,[16,18] which also confers resistance to TXA707 (MIC >64 μg mL^{-1}) but occurs less frequently than the G196S mutation.[4] Thus, TXA6101 retains significant activity against FtsZ mutant *S. aureus* strains that are resistant to TXA707. We therefore hypothesized that TXA6101 should be associated with a lower frequency of resistance (FOR) in MRSA MPW020 than TXA707, which we have previously reported to be 4.3×10^{-8}.[5] To this end, we determined the corresponding FOR value for TXA6101 in MPW020 and found it to be 3.6×10^{-9}, approximately 1 order of magnitude lower than that of TXA707 (Table 1).

Table 2. Activities of TXA707 and TXA6101 against MRSA MPW020 Isolates Expressing FtsZ Mutant Proteins[a]

	MIC (μg mL^{-1})	
compound	G196S	G193D
TXA707	>64	>64
TXA6101	1	1

[a]MIC denotes minimal inhibitory concentration.

Crystal Structure of TXA707 in Complex with Wild-Type SaFtsZ. We first determined the crystal structure of the SaFtsZ enzymatic domain (residues 12−316) in complex with TXA707, refined at 1.3 Å resolution. Although no nucleotides or divalent cations were added during the purification or crystallization steps, the crystal structure contains GDP and Ca^{2+} (Figure 2A and Supporting Information Figure S2). Two molecules of compound vehicle (1-methyl-2-pyrrolidone) were found in the crystal structure, one in an inner space between FtsZ and GDP (Supporting Information Figure S2) and the other on the molecular interface between neighboring FtsZ molecules. As summarized in Table 3, the overall structure of SaFtsZ when complexed with TXA707 is essentially the same (rmsd = 0.482 Å for 247 aligned C_α atoms) as that previously reported for the inhibitor-free form of SaFtsZ (PDB entry: 3VOA).[19] The overall structure of SaFtsZ when complexed with TXA707 is also similar (rmsd = 0.330 Å for 230 aligned C_α atoms) to the previously reported structure of SaFtsZ in complex with the FtsZ-targeting benzamide PC190723 (Supporting Information Figure S1) (PDB entry: 4DXD).[15]

A difference Fourier omit map clearly demonstrates that TXA707 binds to an intersubdomain pocket similar to that occupied by PC190723, with the protein interactions around the benzamide moiety of the two compounds being mostly conserved (Figure 2A and Supporting Information Figure S3A). However, there is a notable difference in the

DOI: 10.1021/acschembio.7b00323
ACS Chem. Biol. 2017, 12, 1947−1955

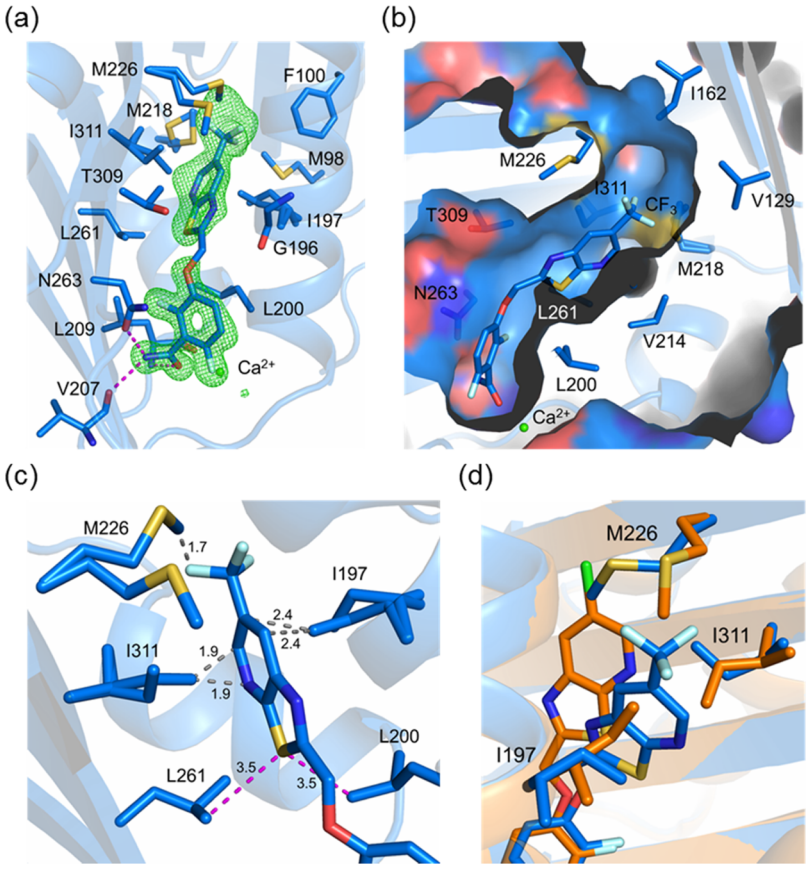

Figure 2. TXA707 in complex with wild-type SaFtsZ. (a) Expanded view of the TXA707 binding site, with the $F_0 - F_c$ omit map (green) being contoured at 3.0σ. The hydrogen bonds are depicted as dashed magenta lines. (b) Molecular surface of the binding pocket. (c) Expanded view highlighting the interactions of the CF_3-substituted thiazolopyridine ring with the protein. The alternative conformers of Ile197, Met226, and Ile311 are shown. Steric clashes and hydrophobic contacts are indicated by gray and magenta dashed lines, respectively. The indicated distances are in Å. (d) Superposition with the PC190723−SaFtsZ complex (orange, PDB entry: 4DXD). The major conformers are shown as in (b).

Table 3. Values of rmsd between the C_α Atoms of Each Pair of SaFtsZ Crystal Structures[a]

	TXA707 wild-type	TXA6101 wild-type	TXA6101 G196S	G196S	PDB: 3VOA	PDB: 3VOB	PDB: 4DXD
TXA707 wild-type	--	0.169 (243)	0.260 (238)	0.499 (259)	0.482 (247)	0.356 (246)	0.330 (230)
TXA6101 wild-type		--	0.198 (255)	0.529 (290)	0.530 (282)	0.366 (269)	0.307 (249)
TXA6101 G196S			--	0.491 (271)	0.543 (267)	0.393 (259)	0.296 (239)
G196S				--	0.234 (278)	0.344 (286)	0.330 (278)
PDB: 3VOA					--	0.285 (279)	0.368 (284)
PDB: 3VOB						--	0.297 (272)
PDB: 4DXD							--

[a]Values in parentheses reflect the number of aligned C_α atoms. rmsd denotes root-mean-square deviation.

conformations of the two compounds in the target site of the protein. TXA707 adopts a novel "bent" conformation that contrasts the straight conformation adopted by PC190723 (Figure 2B and Supporting Information Figure S3B). The interplanar angles between the fused thiazolopyridine rings and the difluoro-benzamide ring are also significantly different (45° for TXA707 versus 24° for PC190723). The CF_3-substituted thiazolopyridine ring system of TXA707 is sandwiched between Ile197 and Ile311, with the sulfur atom of the thiazole making hydrophobic contacts with the side chains of Leu200 (3.5 Å) and Leu261 (3.5 Å) (Figure 2C). By contrast, the corresponding sulfur atom of PC190723 interacts with Gly196 and Thr309 (Supporting Information Figure S3A).

Unlike the Cl-substituted thiazolopyridine rings of PC190723, the corresponding CF_3-substituted ring system of TXA707 is accommodated in an inner hydrophobic pocket surrounded by the hydrophobic residues Met98, Phe100, Val129, Ile162, Gly193, Ile197, Val214, Met218, Met226, Leu261, and Ile311 (Figure 2A,B). This pocket appears unique to the TXA707−SaFtsZ complex, as it was not observed in previous structures of inhibitor-free SaFtsZ and SaFtsZ in complex with PC190723.[15,19] In both previously reported structures, the side chains of Ile197, Met226, and Ile311 block access to the inner hydrophobic pocket (Supporting Information Figure S3B,C). TXA707 binding to SaFtsZ induces conformational changes of the side chains of Ile197, Met226, and Ile311 that open up the hydrophobic pocket to accommodate the CF_3-substituted thiazolopyridine rings (Figure 2D). During the initial refinement, positive differences in the Fourier map appeared in the residues surrounding

DOI: 10.1021/acschembio.7b00323
ACS Chem. Biol. 2017, 12, 1947−1955

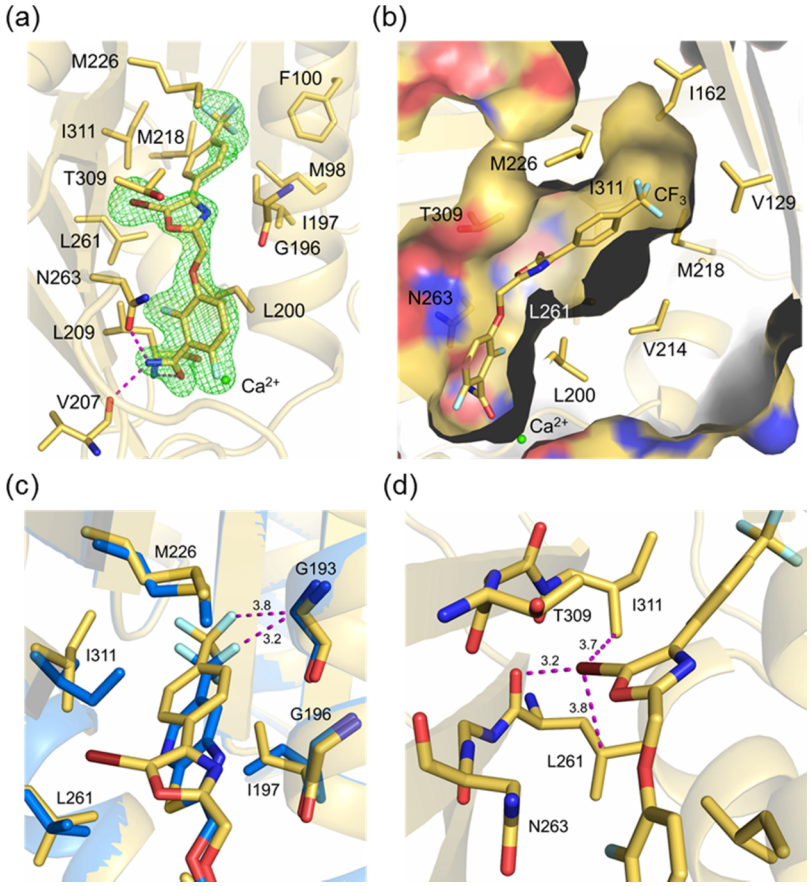

Figure 3. TXA6101 in complex with wild-type SaFtsZ. (a) Expanded view of the TXA6101 binding site, with the $F_0 - F_c$ omit map (green) being contoured at 3.0σ. The hydrogen bonds are depicted as dashed magenta lines. (b) Molecular surface of the binding pocket. (c) Superposition with the TXA707−SaFtsZ complex (blue). The distances between the CF_3 group of each compound and the C_α atom of Gly193 (depicted by the magenta dashed lines) are indicated in Å. (d) Expanded view highlighting the interactions between the bromo group of TXA6101 and the protein. Hydrophobic contacts are depicted by magenta dashed lines, with the indicated distances being in Å.

TXA707, and the alternative conformations of Ile197, Met226, and Ile311 were built into this density map. The minor conformers of Ile197, Met226, and Ile311 were very close to TXA707, suggesting that the alternative conformations of the three residues correspond to the presence and absence of the inhibitor. To minimize the positive difference peaks, the occupancy of TXA707 was set to 0.80, whereas those of Ile197, Met226, and Ile311 were set to 0.80 for the TXA707-bound form and 0.20 for the unbound form (Figure 2A). This conformational alternation reflects the structural plasticity of the inhibitor binding pocket of SaFtsZ.

Crystal Structure of TXA6101 in Complex with Wild-Type SaFtsZ. We also determined the crystal structure of the SaFtsZ enzymatic domain in complex with TXA6101, refined at 2.0 Å resolution. No significant differences (rmsd = 0.169 Å for 243 aligned C_α atoms) were observed between the FtsZ structures in the TXA707 and TXA6101 complexes (Table 3). TXA6101 binds to a similar pocket as TXA707 and PC190723,[15,19] with TXA6101 also adopting a bent conformation similar to TXA707 (Figure 3A,B). The CF_3-substituted phenyl ring of TXA6101 is more extended than the corresponding CF_3-substituted thiazolopyridine rings of TXA707 and is therefore more deeply inserted into the hydrophobic pocket that becomes accessible by the binding-induced conformational changes of the side chains of Ile197, Met226, and Ile311 (Figure 1A,B). As a result, the distance between the nearest fluorine atom of the CF_3 group of TXA6101 and the C_α atom of Gly193 (3.8 Å) is longer than the corresponding distance (3.2 Å) of TXA707 (Figure 3C). The interplanar angle between the oxazole ring and the benzamide ring of TXA6101 is 50°. The bromo group on the oxazole ring of TXA6101 interacts with a hydrophobic pocket formed by the side chains of Leu261, Asn263, Thr309, and Ile311 (Figure 3D). The distances between the bromo group and the carbonyl oxygen of Leu261, the C_γ atom of Leu261, and the $C_{\gamma 2}$ atom of Ile311 are 3.2, 3.8, and 3.7 Å, respectively. These tight contacts significantly serve to fix the orientation of the oxazole ring of TXA6101 in a conformation that is rotated approximately 55° relative to the corresponding thiazolopyridine rings of TXA707. Leu261 interacts with both TXA707 and TXA6101, but the interactions differ: one being with the sulfur atom on the thiazole ring of TXA707 and the other being with the bromo group on the oxazole ring of TXA6101 (Figures 2C and 3C,D).

Crystal Structure of TXA6101 in Complex with G196S Mutant SaFtsZ. Recall that TXA6101 retains activity against MRSA that expresses G196S mutant FtsZ, which confers resistance to TXA707 (Table 2). Thus, in addition to determining the structure of TXA6101 in complex with wild-type SaFtsZ, we also determined the crystal structure of TXA6101 in complex with G196S mutant FtsZ (residues 12−316) at 1.7 Å resolution. The overall structure of the G196S mutant SaFtsZ when complexed with TXA6101 is essentially

DOI: 10.1021/acschembio.7b00323
ACS Chem. Biol. 2017, 12, 1947−1955

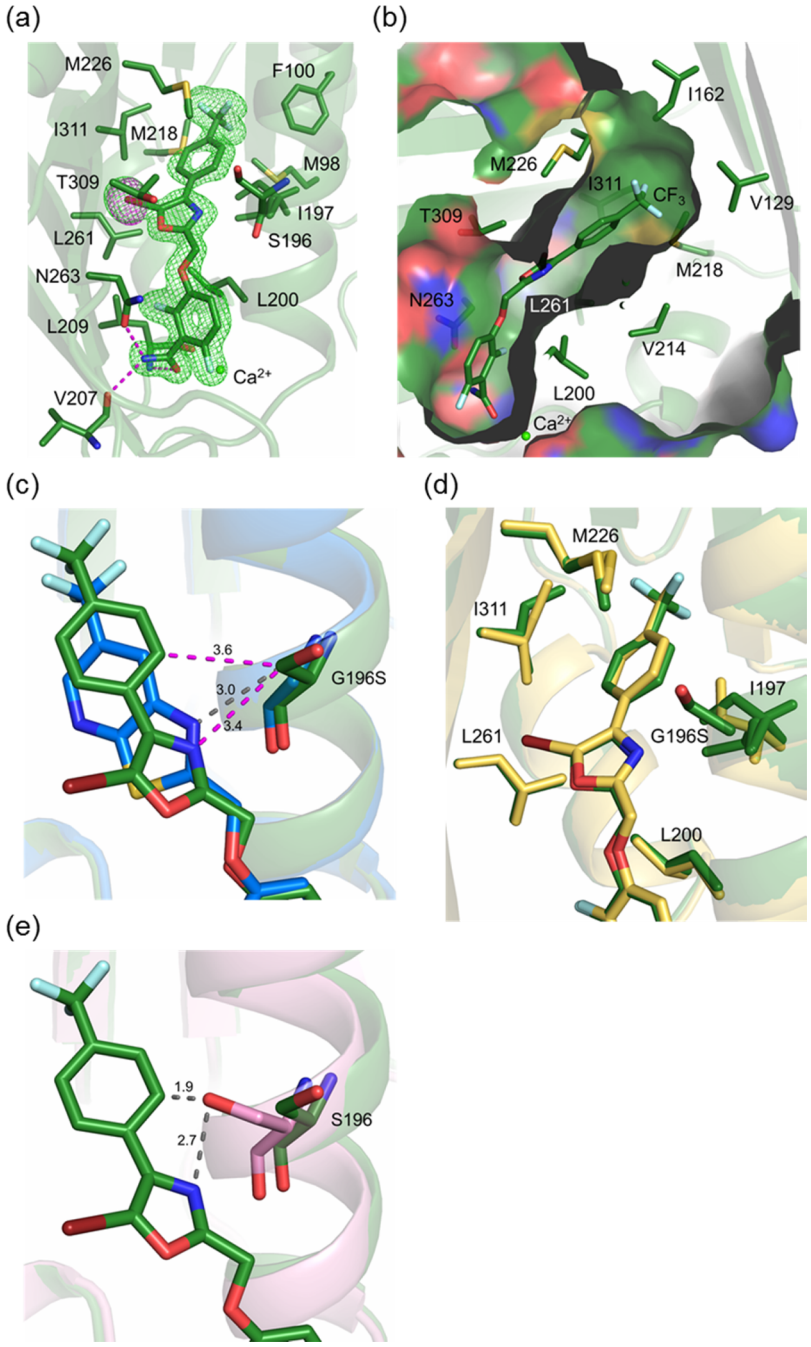

Figure 4. TXA6101 in complex with G196S mutant SaFtsZ. (a) Expanded view of the TXA6101 binding site, with the $F_0 - F_c$ omit map (green) being contoured at 3.0σ. The anomalous difference map (magenta) is contoured at 5.0σ. (b) Molecular surface of the binding pocket. (c) Superposition with the wild-type SaFtsZ-TXA707 complex (blue), with steric clashes and hydrophobic contacts being depicted by gray and magenta dashed lines, respectively. Indicated distances are in Å. (d) Superposition with the wild-type SaFtsZ−TXA6101 complex (yellow). (e) Superposition with the inhibitor-free G196S mutant FtsZ (pink), with steric clashes being depicted by gray dashed lines. Indicated distances are in Å.

the same (rmsd = 0.198 Å for 255 aligned C_α atoms) as that of wild-type SaFtsZ in complex with TXA6101 (Table 3), with the compound binding site being similar in both complexes (Figure 4A,B). As observed in the TXA6101 complex with wild-type SaFtsZ, the bromo group on the oxazole ring of TXA6101 in the G196S SaFtsZ complex interacts with the hydrophobic pocket formed by Leu261, Asn263, Thr309, and Ile311. The CF_3-phenyl and oxazole rings of TXA6101 form contacts with the C_β atom of the Ser196 side chain, enabling the compound to bind the G196S mutant protein (Figure 4C). Superimposition of the G196S−TXA6101 and wild-type−TXA6101 complexes reveals no major structural differences, except for a slight change in the conformation of Ile197 and the orientation of the CF_3-phenyl ring (Figure 4D).

We also determined the crystal structure of inhibitor-free G196S SaFtsZ. This structure shows a greater similarity (rmsd = 0.234 Å for 278 aligned C_α atoms) to the structure of the inhibitor-free wild-type protein (PDB entry: 3VOA) than to the G196S mutant protein in complex with TXA6101 (rmsd = 0.491 Å for 271 aligned C_α atoms), suggesting that the structure of SaFtsZ is less affected by the G196S mutation than by the binding of the inhibitor (Table 3). The only significant

DOI: 10.1021/acschembio.7b00323
ACS Chem. Biol. 2017, 12, 1947−1955

difference between the structures G196S SaFtsZ in the absence and presence of TXA6101 is in the conformation of Ser196, which is rotated in the bound form to avoid steric hindrance with TXA6101 (Figure 4E).

■ DISCUSSION

G196S is the most frequently observed mutation in SaFtsZ that confers resistance to FtsZ-targeting benzamides like TXA707 and PC190723.[4,14−17] In this study, we show that the benzamide derivative TXA6101 retains antistaphylococcal activity against MRSA that expresses G196S mutant FtsZ (Table 2). Our crystallographic results clearly demonstrate that TXA6101 binds to the G196S mutant SaFtsZ tightly (Figure 4A). Detailed inspection of the structure of the G196S−TXA6101 complex suggests that single-bond rotations between the phenyl, oxazole, and benzamide rings of the compound enable it to interact well with surrounding amino acid residues (particularly Ser196) without steric clash (Figure 4C). Unlike the oxazole and phenyl rings of TXA6101, which are linked by a single rotatable bond, the corresponding thiazole and pyridyl rings of TXA707 are fused. As a result, TXA707 cannot avoid a steric clash between the nitrogen atom on the thiazole ring of the compound and Ser196 (Figure 4C). These results suggest that the presence or absence of a single bond linking the five- and six-membered rings determines the ability of the inhibitor to target the G196S mutant protein.

In addition to the G196S mutation, our MIC results indicate that the G193D mutation in SaFtsZ also confers resistance to TXA707 but not to TXA6101 (Table 2). While the G193D mutation has been previously observed in MRSA strains resistant to TXA707 and PC190723, it does not occur as frequently as the G196S mutation.[4,15,16] The CF_3 group in TXA707 is closer to the C_α atom of Gly193 than the corresponding moiety in TXA6101 (Figure 3C). Consequently, the presence of a G193D mutation would result in the bulky side chain of Asp193 causing a steric clash with TXA707, whereas TXA6101 would still be accommodated. Thus, our crystallographic results provide structural explanations for the differential activities of TXA6101 and TXA707 against MRSA strains expressing two different FtsZ mutants. The ability of TXA6101 to retain activity against MRSA strains that express G196S or G193D mutant FtsZ is reflected in the lower FOR of TXA6101 in MRSA relative to that of TXA707 (Table 1). Note that mutations in SaFtsZ residues (e.g., N263 and L200) located in a region of the binding pocket adjacent to the benzamide functionality that is common to TXA707 and TXA6101 (Figures 2 and 3) confer resistance to both agents (MIC > 64 μg mL^{-1}). It is therefore likely that such FtsZ mutations underlie the MRSA FOR of TXA6101.

Our crystallographic results also reveal that both TXA707 and TXA6101 adopt novel bent conformations when bound to SaFtsZ, with the binding of the compounds inducing the formation of an inner hydrophobic pocket that interacts with the CF_3-substituted ring. These structural features were not observed in previously reported crystal structures of SaFtsZ alone or in complex with PC190723.[15,19] The binding of TXA707 and TXA6101 induces conformational rearrangements of Ile197, Met226, and Ile311 that lead to the formation of an inner hydrophobic pocket (Figure 2D), with Met226 acting as a gate that opens up the pocket. The question arises as to why the binding of TXA707 and TXA6101, but not PC190723, induces such conformational rearrangements in SaFtsZ. The sole chemical difference between TXA707 and PC190723 is the presence of a CF_3 group in TXA707 in place of a corresponding chloro group in PC190723 (Figure 1 and Supporting Information Figure S1). The previously reported structure of the PC190723−SaFtsZ complex allows one to infer the impact of replacing the chloro group in PC190723 with a CF_3 group. Such a substitution would generate steric clashes between the compound and residues Gln192, Gly193, and Gly227 (Supporting Information Figure S3A). To avoid such steric clashes, the movement of the side chain of Met226 leads to a series of conformational rearrangements in residues Ile197 and Ile311, as well as in TXA707. These conformational changes are evident in a structural comparison of the TXA707−SaFtsZ and PC190723−SaFtsZ complexes (Figure 2D). Significantly, the space around Met226 permits the movement of the amino acid side chain.

The benzamide ring of TXA707 and TXA6101 likely acts as a hinge point, facilitating the conformational changes of the other rings in the compounds. Benzamide derivatives like PC190723, TXA707, and TXA6101 have been the most intensely studied FtsZ-targeting inhibitors,[4,5,14−16,20,21] and the benzamide ring is structurally stabilized via robust interactions within the binding pocket of SaFtsZ. In this connection, superimposition of the PC190723, TXA707, and TXA6101 complexes with SaFtsZ reveals that the benzamide rings are precisely overlapped (Supporting Information Figure S4). Thus, key factors, which include the avoidance of steric effects, a suitable environment around Met226, and the benzamide ring of the inhibitor acting as a hinge point, play a significant role in the conformational adaptation that accompanies inhibitor binding to SaFtsZ.

Our MIC results shown in Table 1 indicate that the antistaphylococcal activity of TXA6101 (MIC = 0.125 μg mL^{-1}) is 8-fold greater than that of TXA707 (MIC = 1 μg mL^{-1}). The structure of the TXA6101−SaFtsZ complex provides insight into the basis for this differential activity. Inspection of this structure reveals that the bromo group on the oxazole ring of the compound engages in multiple interactions with several hydrophobic side chains and main chains on the rigid β-sheet in the C-terminal subdomain of SaFtsZ (Figure 3D). TXA707 lacks this bromo group (Figure 1). In addition, our MIC results show that the antistaphylococcal activity of TXD1122 (MIC = 4 μg mL^{-1}), a compound identical to TXA6101 but lacking the bromo group (Supporting Information Figure S1), is 32-fold lower than that of TXA6101 and 4-fold lower than that of TXA707 (Table 1). Thus, the extensive interactions of the bromo group of TXA6101 play an important role in enhancing both the SaFtsZ-targeting affinity and the antistaphylococcal activity of the compound relative to TXA707. Future studies will be directed at assessing the antistaphylococcal efficacy of TXA6101 *in vivo*.

The novel hydrophobic pocket we have identified in our studies offers the possibility of further structural optimization of the inhibitors. Within this hydrophobic pocket, extra space still remains around the CF_3 group of TXA707 and TXA6101 (Figures 2B, 3B, and 4B). The possibility of a binding site extension along the intersubdomain cleft has been previously suggested by molecular dynamics studies with large fluorescent analogues of PC190723.[22] The newly identified hydrophobic pocket in SaFtsZ and increased structural flexibility of the inhibitor are key factors for overcoming drug resistance mutations in the protein and offer a structural basis for the design of new FtsZ inhibitors with enhanced antibacterial potency and a reduced susceptibility to mutational resistance.

DOI: 10.1021/acschembio.7b00323
ACS Chem. Biol. 2017, 12, 1947−1955

Table 4. Data Collection and Refinement Statistics for the $SaFtsZ_{12-316}$ Crystal Structures

data set	TXA707 wild-type	TXA6101 wild-type	TXA6101 G196S	G196S
PDB entry	5XDT	5XDU	5XDV	5XDW
Data Collection				
X-ray source	SPring-8 BL44XU	SPring-8 BL32XU	SPring-8 BL44XU	SPring-8 BL44XU
wavelength (Å)	0.900	1.100	0.900	0.900
space group	*C*2	*C*2	*C*2	*C*2
Unit-Cell Parameters				
a, *b*, *c* (Å)	70.55, 51.19, 86.45	70.76, 51.57, 86.66	71.39, 50.44, 88.26	71.76, 51.01, 88.33
β (deg)	108.68	108.75	109.97	110.71
resolution (Å)[a]	50.0−1.30 (1.32−1.30)	50.0−2.00 (2.03−2.00)	50.0−1.70 (1.73−1.70)	50.0−2.00 (2.03−2.00)
total reflections	503 253	55 580	121 237	110 946
unique reflections	71 548	19 640	32 355	20 347
completeness (%)	99.5 (100.0)	97.7 (98.3)	99.5 (100.0)	99.7 (99.8)
I/σ	41.7 (2.2)	13.6 (2.6)	27.7 (2.7)	17.6 (2.9)
R_{merge} (%)[b]	4.9 (76.0)	8.1 (26.4)	6.0 (36.8)	14.6 (87.9)
$CC_{1/2}$ (%)	(84.1)	(89.8)	(89.7)	(79.1)
Refinement				
resolution (Å)	41.0−1.30	40.9−2.00	41.5−1.70	41.3−2.00
R_{work}/R_{free} (%)[c]	13.6/16.8	20.1/23.9	17.3/20.6	18.8/23.6
no. of chains in the asymmetric unit	1	1	1	1
No. of Atoms				
protein	2393	2211	2230	2213
ligand	69	58	58	29
water	304	168	219	168
Average B-Factors (Å^2)				
protein	24.8	32.3	28.4	24.7
ligand	23.8	29.9	22.9	16.7
water	39.1	37.2	37.1	30.3
rmsd from Ideal				
bond length (Å)	0.011	0.012	0.012	0.010
bond angle (deg)	1.746	1.578	1.735	1.448
Ramachandran Plot				
favored	334 (98.2%)	294 (96.7%)	303 (98.4%)	299 (98.4%)
allowed	6 (1.8%)	10 (3.3%)	5 (1.6%)	5 (1.6%)
outlier	0 (0%)	0 (0%)	0 (0%)	0 (0%)

[a]Values in parentheses are for the highest resolution shells. [b]$R_{merge} = \sum_{hkl}\sum_i|I_i(hkl) - \langle I(hkl)\rangle|/\sum_{hkl}\sum_i I_i(hkl)$, where $I_i(hkl)$ is the intensity of an individual reflection and $\langle I(hkl)\rangle$ is the mean intensity of symmetry-equivalent reflections. [c]$R_{work} = \sum_{hkl}||F_{obs}| - |F_{calc}||/\sum_{hkl}|F_{obs}|$, where F_{obs} and F_{calc} are the observed and calculated structure-factor amplitudes, respectively. R_{free} was calculated in the same manner as R_{work} but using only a 5% unrefined subset of the reflection data.

METHODS

Bacterial Strains and Compounds. MRSA MPW020 was isolated from a patient blood sample at Robert Wood Johnson University Hospital in New Brunswick, NJ, and provided by Melvin P. Weinstein (Rutgers Robert Wood Johnson Medical School, New Brunswick, NJ). The selection and characterization of the two FtsZ mutant strains of MPW020 (G196S and G193D) are described elsewhere.[5] Briefly, MRSA MPW020 was plated on tryptic soy agar (TSA) plates containing 4 μg mL^{-1} of TXA707, and resistant colonies that emerged were isolated. The *ftsZ* gene of each isolate was sequenced to identify the mutation. TXA707 was synthesized as previously described.[4] TXA6101 and TXD1122 were synthesized as described in the Supporting Information.

Minimal Inhibitory Concentration (MIC) Assays. Microdilution assays to determine the MIC of each compound were conducted according to Clinical and Laboratory Standards Institute (CLSI) guidelines.[23] In the MIC assays, log-phase bacteria were added to 96-well microtiter plates (at 5×10^5 CFU mL^{-1}) containing 2-fold serial dilutions of the compound in 0.1 mL of cation-adjusted Mueller−Hinton (CAMH) broth, with each compound concentration being present in duplicate. The MIC is defined as the lowest compound concentration at which growth is ≥90% inhibited after 18−24 h of incubation at 37 °C.

Assay for Determining the Frequency of Resistance (FOR). The FOR of MPW020 to TXA6101 was determined using a previously established large inoculum approach.[5] In this approach, a large inoculum of MPW020 bacteria was spread on TSA plates containing 2 μg mL^{-1} TXA6101. The plates were incubated at 37 °C and examined after 48 h. FOR was calculated from the ratio of the number of colonies observed on the selective plates to the total number of plated bacteria.

SaFtsZ Expression and Purification. The enzymatic domain of the *S. aureus ftsZ* gene (12−316) was amplified from the *SaftsZ*-pColdI plasmid we have described previously[24] using KOD-Plus-DNA polymerase (TOYOBO) and the following primers: 5′-G_2TAG_2C-$ATATG_2CGACT_3A_3G_2TCAT_2G_2TGTAG_2TG_2$-3′ in the forward direction and 5′-$GA_2T_2CG_2ATC_2T_2A_2TCA_4C_2AGT_2GCA_2TA_2CT$-$GT_2ACA_2CA_2TCTC$-3′ in the reverse direction. The amplified sequence was then subcloned into a modified pColdI vector whose Factor Xa protease site (IEGR) was replaced with a TEV protease site (LQENLYFQG), resulting in the addition of residues MNHKVHHH-HHHLQENLYFQGHM before the Ala12 residue at the N-terminus of SaFtsZ. The resulting plasmid was then transformed into *E. coli* DH5α and extracted using the QIAprep spin miniprep kit (QIAGEN).

DOI: 10.1021/acschembio.7b00323
ACS Chem. Biol. 2017, 12, 1947−1955

Plasmids with the appropriate sequence were than transformed into *E. coli* strain BL21(DE3), and the cells were cultured in LB medium with 100 mg L^{-1} ampicillin at 37 °C until the optical density at 600 nm reached 0.5. After the addition of 0.5 mM IPTG, cultivation was continued for an additional 24 h at 15 °C. Cells were harvested by centrifugation for 20 min at 9000*g* and 4 °C and then stored at −80 °C.

For protein extraction and purification, the cell pellets were resuspended in lysis buffer (50 mM Tris-HCl pH 7.5, 300 mM NaCl, 20 mM imidazole) and lysed with an EmulsiFlex-C3 homogenizer (Avestin). The suspension was ultracentrifuged for 30 min at 100 000*g* and 4 °C. The supernatant was filtered using a 0.45 μm syringe filter (Sartorius) and loaded onto a 5 mL HisTrap HP column (GE Healthcare). The protein was eluted by a 45−310 mM imidazole gradient. Fractions containing the desired protein were dialyzed against dialysis buffer (50 mM Tris-HCl pH 7.5) for 3 h at 4 °C. The His-tag was then removed by overnight digestion at room temperature in the presence of 1 mg of His-tagged TEV protease and 1 mM DTT. The residual sequences after the digestion are GHM. The mixture was then loaded onto a HisTrap HP column, and the flow-through fraction was collected and diluted 10-fold in dialysis buffer. The resulting solution was then loaded onto a 1 mL Resource Q column (GE Healthcare), and the protein was eluted by a 30−750 mM NaCl gradient. The FtsZ fractions were further purified using a HiLoad 16/600 Superdex 200 prep-grade column (GE Healthcare) equilibrated with gel-filtration buffer (20 mM Tris-HCl pH 7.5, 150 mM NaCl). The purity of the protein was confirmed by SDS-PAGE. The purified protein was concentrated to approximately 5 mg mL^{-1} with a Vivaspin 20−10K concentrator (GE Healthcare), flash-frozen in liquid nitrogen, and immediately stored at −80 °C.

G196S mutant $SaFtsZ_{12-316}$ was cloned, expressed, and purified as described above, with the exception that site-directed mutagenesis was performed by inverse-PCR using the following primers: 5′-CCAAGGTGTACAAaGTATCTCAGACTTAATCG-3′ in the forward direction and 5′-CGATTAAGTCTGAGATACtTTGTACACCTTGG-3′ in the reverse direction. The altered nucleotides in these primers are indicated by lower case letters, and the codons corresponding to the amino acid residues to be altered are underlined.

Crystallization, Data Collection, and Structure Determination. The SaFtsZ crystals in this study were obtained using the sitting-drop vapor-diffusion technique at 20 °C in reservoir conditions based on JBScreen pentaerythritol 2 (Jena Bioscience). All $SaFtsZ_{12-316}$−inhibitor complexes were crystallized using a soaking method. For the complex of TXA707 with wild-type SaFtsZ, the protein was crystallized at 9.4 mg mL^{-1} under conditions of 100 mM Tris-HCl pH 7.6, 41% (w/v) pentaerythritol propoxylate 629 (PEP629), and 300 mM KCl. After 2 months, the crystal was soaked in the same reservoir supplemented with 5 mM TXA707 and 10% (v/v) 1-methyl-2-pyrrolidone for 2 days. For the complex of TXA6101 with wild-type SaFtsZ, the protein was crystallized at 9.4 mg mL^{-1} under conditions of 100 mM Tris-HCl pH 7.8, 43% (w/v) PEP629, and 300 mM KCl. After 3 weeks, the crystal was soaked in the same reservoir supplemented with 2 mM TXA6101 and 2% (v/v) DMSO for 1 day. For the complex of TXA6101 with G196S mutant SaFtsZ, the protein was crystallized at 4.4 mg mL^{-1} under conditions of 100 mM Tris-HCl pH 8.4, 43% (w/v) PEP629, and 300 mM KCl. After 4 months, the crystal was soaked in the same reservoir supplemented with 5 mM TXA6101 and 10% (v/v) DMSO for 3 days. The inhibitor-free form of G196S mutant SaFtsZ was crystallized at 4.5 mg mL^{-1} under conditions of 100 mM Tris-HCl pH 8.5, 45% (w/v) PEP629, and 300 mM KCl. Crystals were flash-frozen in a stream of nitrogen at −180 °C without cryoprotectants after being mounted in a loop. X-ray diffraction data were collected at SPring-8 BL44XU and BL32XU (Hyogo, Japan) under cryogenic conditions. The diffraction data were processed and scaled with HKL2000.[25] The phases were determined by molecular replacement with Phaser in the CCP4 suite[26] using a previous SaFtsZ−GDP structure (PDB entry: 3VOA)[19] as a search model. The model structures were refined with Refmac5[27] and PHENIX,[28] with manual modification using COOT.[29] The refined structures were validated with MolProbity.[30] Data collection and refinement statistics are summarized in Table 4. The final atomic coordinates and structure factor amplitudes were deposited in the RCSB Protein Data Bank (PDB entries: 5XDT, 5XDU, 5XDV, and 5XDW). Interplanar angles were calculated using UCSF Chimera,[31] and figures were prepared with PyMOL (www.pymol.org).

■ ASSOCIATED CONTENT

Supporting Information

The Supporting Information is available free of charge on the ACS Publications website at DOI: 10.1021/acschembio.7b00323.

Additional experimental methods; chemical structures of TXD1122 and PC190723; expanded view of the GDP binding site of wild-type SaFtsZ in complex with TXA707; previous crystal structures of wild-type SaFtsZ; superposition of the crystal structures of TXA707, TXA6101, and PC190723 in complex with SaFtsZ (PDF)

■ AUTHOR INFORMATION

Corresponding Authors

*E-mail: pilchds@rwjms.rutgers.edu (D.S.P.).
*E-mail: h-matsu@fc.ritsumei.ac.jp (H.M.).

ORCID

Hiroyoshi Matsumura: 0000-0003-0361-3796

Notes

The authors declare the following competing financial interest(s): Drs. Pilch and LaVoie are co-founders of TAXIS Pharmaceuticals and therefore have a financial interest in the company.

#D.S.P. and H.M. jointly supervised this work.

■ ACKNOWLEDGMENTS

We thank the staff of the SPring-8 BL44XU and BL32XU beamline for their assistance with the collection of the X-ray diffraction data. We are also indebted to Melvin P. Weinstein (Rutgers Robert Wood Johnson Medical School, New Brunswick, NJ) for providing MRSA clinical isolate MPW020. This work was supported by National Institutes of Health grant RO1 AI118874 (to D.S.P.); a Grant-in-Aid from the Japan Society for the Promotion of Science (JSPS) (Fellows Grant 15J00589 to J.F.); Grants-in-Aid for Scientific Research (24109017 to T.I. and 15H04443, 26102526, 16H00783, and 17H05732 to H.M.); the Science Research Promotion Fund from the Promotion and Mutual Aid Corporation for Private Schools of Japan; the Futaba Electronics Memorial Foundation; and the Cooperative Research Program of Institute for Protein Research, Osaka University (CR-16-05 and CR-17-05). This work was performed under the approval of the Photon Factory and SPring-8 Program Advisory Committee (proposals 2016R-68, 2016G658, 2014A6947, 2014B6947, 2015A6538, 2015B6538, 2016A6639, 2016B6639, 2016A2572, and 2016B2572).

■ ABBREVIATIONS

MIC, minimum inhibitory concentration; FOR, frequency of resistance; MRSA, methicillin-resistant *Staphylococcus aureus*; SaFtsZ, *Staphylococcus aureus* FtsZ; CAMH, cation-adjusted Mueller−Hinton; LB, Luria−Bertani; DTT, dithiothreitol; rmsd, root-mean-square deviation; IPTG, isopropyl β-D-1-thiogalactopyranoside; PEP629, pentaerythritol propoxylate

DOI: 10.1021/acschembio.7b00323
ACS Chem. Biol. 2017, 12, 1947−1955

629; TSA, tryptic soy agar; TEV, tobacco etch virus; DMSO, dimethyl sulfoxide

REFERENCES

(1) (2013) *Antibiotic Resistance Threats in the United States 2013*, Centers for Disease Control and Prevention, Atlanta, GA.

(2) (2014) *Report to the President on Combating Antibiotic Resistance*, President's Council of Advisors on Science and Technology, Washington, DC.

(3) (2014) *Antimicrobial Resistance: Global Report on Surveillance*, World Health Organization, Geneva, Switzerland.

(4) Kaul, M., Mark, L., Zhang, Y., Parhi, A. K., Lyu, Y. L., Pawlak, J., Saravolatz, S., Saravolatz, L. D., Weinstein, M. P., LaVoie, E. J., and Pilch, D. S. (2015) TXA709, an FtsZ-Targeting Benzamide Prodrug with Improved Pharmacokinetics and Enhanced *In Vivo* Efficacy against Methicillin-Resistant *Staphylococcus aureus*. *Antimicrob. Agents Chemother. 59*, 4845−4855.

(5) Kaul, M., Mark, L., Parhi, A. K., LaVoie, E. J., and Pilch, D. S. (2016) Combining the FtsZ-Targeting Prodrug TXA709 and the Cephalosporin Cefdinir Confers Synergy and Reduces the Frequency of Resistance in Methicillin-Resistant *Staphylococcus aureus*. *Antimicrob. Agents Chemother. 60*, 4290−4296.

(6) Bi, E. F., and Lutkenhaus, J. (1991) FtsZ ring structure associated with division in *Escherichia coli*. *Nature 354*, 161−164.

(7) Adams, D. W., and Errington, J. (2009) Bacterial Cell Division: Assembly, Maintenance and Disassembly of the Z ring. *Nat. Rev. Microbiol. 7*, 642−653.

(8) Erickson, H. P., Anderson, D. E., and Osawa, M. (2010) FtsZ in Bacterial Cytokinesis: Cytoskeleton and Force Generator All in One. *Microbiol. Mol. Biol. Rev. 74*, 504−528.

(9) Awasthi, D., Kumar, K., and Ojima, I. (2011) Therapeutic Potential of FtsZ Inhibition: A Patent Perspective. *Expert Opin. Ther. Pat. 21*, 657−679.

(10) Schaffner-Barbero, C., Martin-Fontecha, M., Chacón, P., and Andreu, J. M. (2012) Targeting the Assembly of Bacterial Cell Division Protein FtsZ with Small Molecules. *ACS Chem. Biol. 7*, 269−277.

(11) Sass, P., and Brötz-Oesterhelt, H. (2013) Bacterial Cell Division as a Target for New Antibiotics. *Curr. Opin. Microbiol. 16*, 522−530.

(12) Li, X., and Ma, S. (2015) Advances in the discovery of novel antimicrobials targeting the assembly of bacterial cell division protein FtsZ. *Eur. J. Med. Chem. 95*, 1−15.

(13) Hurley, K. A., Santos, T. M., Nepomuceno, G. M., Huynh, V., Shaw, J. T., and Weibel, D. B. (2016) Targeting the Bacterial Division Protein FtsZ. *J. Med. Chem. 59*, 6975−6998.

(14) Haydon, D. J., Stokes, N. R., Ure, R., Galbraith, G., Bennett, J. M., Brown, D. R., Baker, P. J., Barynin, V. V., Rice, D. W., Sedelnikova, S. E., Heal, J. R., Sheridan, J. M., Aiwale, S. T., Chauhan, P. K., Srivastava, A., Taneja, A., Collins, I., Errington, J., and Czaplewski, L. G. (2008) An inhibitor of FtsZ with potent and selective anti-staphylococcal activity. *Science 321*, 1673−1675.

(15) Tan, C. M., Therien, A. G., Lu, J., Lee, S. H., Caron, A., Gill, C. J., Lebeau-Jacob, C., Benton-Perdomo, L., Monteiro, J. M., Pereira, P. M., Elsen, N. L., Wu, J., Deschamps, K., Petcu, M., Wong, S., Daigneault, E., Kramer, S., Liang, L., Maxwell, E., Claveau, D., Vaillancourt, J., Skorey, K., Tam, J., Wang, H., Meredith, T. C., Sillaots, S., Wang-Jarantow, L., Ramtohul, Y., Langlois, E., Landry, F., Reid, J. C., Parthasarathy, G., Sharma, S., Baryshnikova, A., Lumb, K. J., Pinho, M. G., Soisson, S. M., and Roemer, T. (2012) Restoring Methicillin-Resistant *Staphylococcus aureus* Susceptibility to Beta-Lactam Antibiotics. *Sci. Transl. Med. 4*, 126ra35.

(16) Stokes, N. R., Baker, N., Bennett, J. M., Berry, J., Collins, I., Czaplewski, L. G., Logan, A., Macdonald, R., Macleod, L., Peasley, H., Mitchell, J. P., Nayal, N., Yadav, A., Srivastava, A., and Haydon, D. J. (2013) An Improved Small-Molecule Inhibitor of FtsZ with Superior *In Vitro* Potency, Drug-Like Properties, and *In Vivo* Efficacy. *Antimicrob. Agents Chemother. 57*, 317−325.

(17) Adams, D. W., Wu, L. J., and Errington, J. (2016) A Benzamide-Dependent *ftsZ* Mutant Reveals Residues Crucial for Z-ring Assembly. *Mol. Microbiol. 99*, 1028−1042.

(18) Stokes, N. R., Baker, N., Bennett, J. M., Chauhan, P. K., Collins, I., Davies, D. T., Gavade, M., Kumar, D., Lancett, P., Macdonald, R., Macleod, L., Mahajan, A., Mitchell, J. P., Nayal, N., Nayal, Y. N., Pitt, G. R., Singh, M., Yadav, A., Srivastava, A., Czaplewski, L. G., and Haydon, D. J. (2014) Design, Synthesis and Structure-Activity Relationships of Substituted Oxazole-Benzamide Antibacterial Inhibitors of FtsZ. *Bioorg. Med. Chem. Lett. 24*, 353−359.

(19) Matsui, T., Yamane, J., Mogi, N., Yamaguchi, H., Takemoto, H., Yao, M., and Tanaka, I. (2012) Structural reorganization of the bacterial cell-division protein FtsZ from *Staphylococcus aureus*. *Acta Crystallogr., Sect. D: Biol. Crystallogr. 68*, 1175−1188.

(20) Kaul, M., Mark, L., Zhang, Y., Parhi, A. K., LaVoie, E. J., and Pilch, D. S. (2013) Pharmacokinetics and *in Vivo* Antistaphylococcal Efficacy of TXY541, a 1-Methylpiperidine-4-Carboxamide Prodrug of PC190723. *Biochem. Pharmacol. 86*, 1699−1707.

(21) Kaul, M., Mark, L., Zhang, Y., Parhi, A. K., LaVoie, E. J., and Pilch, D. S. (2013) A FtsZ-Targeting Prodrug with Oral Antistaphylococcal Efficacy *In Vivo*. *Antimicrob. Agents Chemother. 57*, 5860−5869.

(22) Artola, M., Ruíz-Avila, L. B., Ramírez-Aportela, E., Martínez, R. F., Araujo-Bazán, L., Vázquez-Villa, H., Martín-Fontecha, M., Oliva, M. A., Martín-Galiano, A. J., Chacón, P., et al. (2017) The structural assembly switch of cell division protein FtsZ probed with fluorescent allosteric inhibitors. *Chemical Science 8*, 1525−1534.

(23) (2015) *Methods for Dilution Antimicrobial Sucseptibility Tests for Bacteria That Grow Aerobically*, Approved Standard-Tenth Edition, CLSI Document M07-A10, Clinical and Laboratory Standards Institute, Wayne, PA.

(24) Fujita, J., Maeda, Y., Nagao, C., Tsuchiya, Y., Miyazaki, Y., Hirose, M., Mizohata, E., Matsumoto, Y., Inoue, T., Mizuguchi, K., and Matsumura, H. (2014) Crystal Structure of FtsA from *Staphylococcus aureus*. *FEBS Lett. 588*, 1879−1885.

(25) Otwinowski, Z., and Minor, W. (1997) Processing of X-ray diffraction data collected in oscillation mode. *Methods Enzymol. 276*, 307−326.

(26) McCoy, A. J., Grosse-Kunstleve, R. W., Adams, P. D., Winn, M. D., Storoni, L. C., and Read, R. J. (2007) Phaser crystallographic software. *J. Appl. Crystallogr. 40*, 658−674.

(27) Murshudov, G. N., Skubak, P., Lebedev, A. A., Pannu, N. S., Steiner, R. A., Nicholls, R. A., Winn, M. D., Long, F., and Vagin, A. A. (2011) REFMAC5 for the refinement of macromolecular crystal structures. *Acta Crystallogr., Sect. D: Biol. Crystallogr. 67*, 355−367.

(28) Adams, P. D., Afonine, P. V., Bunkoczi, G., Chen, V. B., Davis, I. W., Echols, N., Headd, J. J., Hung, L. W., Kapral, G. J., Grosse-Kunstleve, R. W., McCoy, A. J., Moriarty, N. W., Oeffner, R., Read, R. J., Richardson, D. C., Richardson, J. S., Terwilliger, T. C., and Zwart, P. H. (2010) PHENIX: a comprehensive Python-based system for macromolecular structure solution. *Acta Crystallogr., Sect. D: Biol. Crystallogr. 66*, 213−221.

(29) Emsley, P., and Cowtan, K. (2004) Coot: model-building tools for molecular graphics. *Acta Crystallogr., Sect. D: Biol. Crystallogr. 60*, 2126−2132.

(30) Chen, V. B., Arendall, W. B., III, Headd, J. J., Keedy, D. A., Immormino, R. M., Kapral, G. J., Murray, L. W., Richardson, J. S., and Richardson, D. C. (2010) MolProbity: all-atom structure validation for macromolecular crystallography. *Acta Crystallogr., Sect. D: Biol. Crystallogr. 66*, 12−21.

(31) Pettersen, E. F., Goddard, T. D., Huang, C. C., Couch, G. S., Greenblatt, D. M., Meng, E. C., and Ferrin, T. E. (2004) UCSF Chimera–a visualization system for exploratory research and analysis. *J. Comput. Chem. 25*, 1605−1612.

DOI: 10.1021/acschembio.7b00323
ACS Chem. Biol. 2017, 12, 1947−1955